Two-dimensional vector-coupled-mode theory for textured planar waveguides

P. Paddon and Jeff F. Young
Advanced Materials and Process Engineering Laboratory, Department of Physics and Astronomy, 2355 East Mall, University of British Columbia, Vancouver, British Columbia, Canada V6T 1Z4

(Received 12 January 1999; revised manuscript received 6 July 1999)

We develop a model to treat coupling between guided modes in planar dielectric waveguides that have been textured in two dimensions with a thin surface grating. The formulation is based on a general Green's-function technique that self-consistently determines the field in the surface grating due to the polarization there. With simplifying approximations, this formalism is cast into a two-dimensional (2D) vector-coupled-mode theory that is more computationally efficient, and that gives considerable insight into the nature of mode coupling in 2D textured structures. These models are applied, by way of example, to illustrate some interesting properties of leaky and bound modes that are coupled together by 2D periodic texture. In particular we discuss the complex photonic band structure describing the dispersion, lifetimes, and polarization properties of the resonant states associated with the textured waveguide. In our analysis we emphasize the fundamental differences between coupling in 2D textured waveguides and infinite 2D photonic crystals. We also show that the vector-coupled-mode theory agrees well with the self-consistent formulation.

I. INTRODUCTION

Surface gratings and slab waveguides each represent fundamental building blocks of many important optical components, instruments, and systems. Although diffraction gratings have been studied for almost a century, interesting applications and fresh understanding of their myriad properties are constantly being developed. Recent work has considered the influence of resonant modes on the specular scattering properties of both one-dimensional (1D) and two-dimensional (2D) gratings formed on the surface of planar, or ''slab,'' waveguide structures.[1,2] It has been noted that the specular reflectivity always reaches 100% in the vicinity of phase-matched excitation of slab modes; this has been considered the possible basis of high-efficiency notch filters. The peculiar Fano-like line shape has been analyzed in some detail,[3,4] and, with the use of 2D gratings, polarization-insensitive filters may be achieved.[5] Most if not all of this body of work has, appropriately, approached the problem as a resonantly enhanced diffraction process.

On the other hand, considering the properties of slab waveguide modes as they are modified by the presence of surface diffraction gratings gives an alternate perspective on the same physical system. In one dimension, slab modes with wave vectors at the Brillouin-zone boundaries become coupled through interaction with the grating.[6] Indeed, one of the most important components of optical communications systems is the distributed feedback (DFB) laser, which owes its superior performance to the renormalized slab modes, or photonic eigenstates, that are created in waveguides containing 1D interface gratings. It was noted early on that for DFB lasers incorporating second-order gratings, the eigenstates of the textured waveguide at the second Brillouin-zone boundary, in general, contain a component of polarization that radiates into the vacuum.[7] The connection with the resonantly enhanced diffraction process mentioned above is that for appropriately phase-matched plane waves incident from the vacuum onto such structures, these renormalized ''leaky'' modes are excited. The polelike response results in the 100% reflection for a particular excitation condition near resonance.

Given the success of the DFB laser, it is then natural to consider the properties of slab waveguides as they are modified by 2D gratings. This viewpoint is intimately related to the topic of two-dimensional photonic band-gap structures in planar waveguide geometries. Interest in slab waveguides, in which a 2D periodic grating pattern is etched to a depth comparable to or exceeding the thickness of the waveguide, has been stimulated by theoretical work[8–10] and the successful experimental demonstration of photonic band-gap structures at microwave[11] and more recently near-infrared[12] wavelengths. To open up a true photonic band gap, a range of frequencies within which it is impossible for light to propagate in any direction, regardless of polarization, one uses 2D or 3D periodically textured dielectrics with large dielectric contrast. Several optoelectronic applications have been suggested for such structures if they can be realized with lattice constants of from 150 to 500 nm in semiconductor hosts.[13–15]

Many of these potential applications assume that a strong 2D periodic scattering potential will modify the dispersion of slab modes in much the same way that infinitely long dielectric cylinders or holes in a dielectric block are known to modify the dispersion of plane waves in 2D photonic crystals. However, the lack of translational invariance perpendicular to the textured plane in these porous waveguides fundamentally alters the nature of the corresponding photonic eigenstates. In particular, the excitations of porous waveguides are manifestly vector fields that cannot be generated from a single scalar field. In addition, even if the 2D textured slab is infinite in extent, some of the resonant excitation modes are lossy, and therefore their band structure is quite generally complex rather than purely real.

We have studied the properties of these waveguide-based 2D photonic crystal structures both experimentally and numerically.[16] There we calculated the specular reflectivity from the porous waveguide, and used the Fano-like resonant features that peak at 100% reflectivity to identify the leaky eigenstates of the structure. To handle the extreme nature of the dielectric texture, which consisted of a free-standing slab completely penetrated by a 2D array of air holes, it was necessary to employ a numerically-intensive algorithm that solves the Maxwell equations ''exactly'' on a spatial grid that extends throughout the porous waveguides. The polarization and lifetime properties of the resonant states so identified for a variety of waveguide structures suggested that they can be thought of largely in terms of superpositions of effective TE and TM slab modes characteristic of the average slab waveguide, coupled via the (strong) 2D dielectric crystal potential. This realization prompted us to formulate a simple, heuristic model to describe the eigenstates of 2D periodically textured dielectric slabs.

The model described subsequently in this paper applies rigorously to slab waveguides that have been textured with a thin, 2D surface grating, but many of the results are also expected to apply qualitatively to photonic bandgap structures in the waveguide geometry. Using a Green's-function technique we are able to self-consistently calculate the total field in the grating region. By associating the Fourier components of the total field with the TE and TM slab modes of the untextured structure, our model simplifies to an eigenvalue problem for the complex eigenfrequencies of the resonant eigenstates. Heuristically, one may consider these eigenstates as linear superpositions of the dominant TE and TM slab modes, as one would in conventional 1D coupled-mode theory. All of the texture-induced coupling between these TE and TM slab mode basis states is rigorously accounted for within the Green's-function formalism. The results obtained by applying this model are consistent with the resonant diffraction literature, and the different perspective provides considerable new insight as to the fundamental nature of these excitations.

II. THEORY

A. Self-consistent formulation

In this section we derive a technique for calculating the resonant electromagnetic excitations of a multilayered slab waveguide that has been textured with a thin 2D surface grating, as illustrated in Fig. 1. We use a Green's-function technique to solve self-consistently for the field in the grating region, $0<z<t_g$, due to the polarization there. This leads to a simple set of equations for the in-plane spatial Fourier components of the field in the grating, which may be solved numerically. In Sec. II B we show how to cast the model as an eigenvalue problem in the coupled mode limit.

The macroscopic Maxwell equations are

$$\nabla\cdot\vec{D}=0, \tag{1}$$

$$c\nabla\times\vec{H}-\frac{\partial\vec{D}}{\partial t}=0,$$

$$\nabla\cdot\vec{B}=0,$$

$$c\nabla\times\vec{E}+\frac{\partial\vec{B}}{\partial t}=0.$$

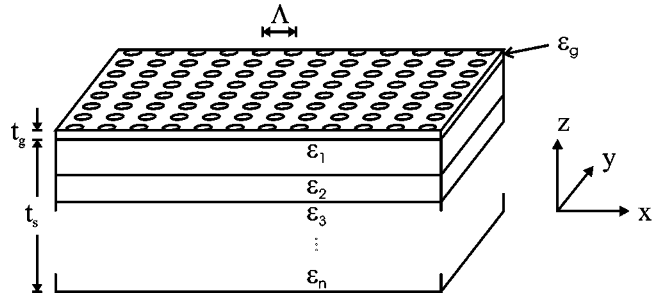

FIG. 1. Schematic of a two-dimensionally textured multilayer slab waveguide.

where, for a nonmagnetic medium,

$$\vec{D}=\vec{E}+4\pi\vec{P}_t,\qquad \vec{H}=\vec{B}. \tag{2}$$

For the planar waveguide geometry depicted in Fig. 1, the total electric dipole moment per unit volume, $\vec{P}_t$, is

$$\vec{P}_t(\vec{r})=\chi_s(z)\vec{E}(\vec{r})+\vec{P}_g(\vec{r}) \tag{3}$$

where $\chi_s(z)$ is the linear susceptibility associated with the various homogeneous layers of the slab waveguide, and $\vec{P}_g(\vec{r})$ is the polarization (to be determined self-consistently) of the grating layer. Thus we are led to solve the inhomogeneous Maxwell equations of the form

$$\begin{aligned}\epsilon_s(z)\nabla\cdot\vec{E}(\vec{r})+\frac{\partial\epsilon_s(z)}{\partial z}\vec{E}(\vec{r})&=-4\pi\nabla\cdot\vec{P}_g(\vec{r})\\ \nabla\times\vec{B}(\vec{r})+i\tilde{\omega}\epsilon_s(z)\vec{E}(\vec{r})&=-4\pi i\tilde{\omega}\vec{P}_g(\vec{r})\\ \nabla\cdot\vec{B}(\vec{r})&=0\\ \nabla\times\vec{E}(\vec{r})-i\tilde{\omega}\vec{B}(\vec{r})&=0,\end{aligned} \tag{4}$$

where the dielectric constant of the multilayer slab is given by

$$\epsilon_s(z)=1+4\pi\chi_s(z), \tag{5}$$

and $\tilde{\omega}=\omega/c$. In this form we see that the polarization in the grating layer acts as a spatially dependent source term in the usual homogeneous equations for a multilayer slab waveguide.

We are primarily interested in cases where the spatial dependence of the grating polarization is periodic in the plane; thus we write

$$\vec{P}_g(\vec{r})=\chi_g(\vec{r})\vec{E}(\vec{r}), \tag{6}$$

and expand the spatial dependence of the linear susceptibility of the grating in a Fourier series as

$$\chi_g(\vec{r})=\sum_m \chi_{\vec{G}_m}(z)\exp(i\vec{G}_m\cdot\vec{\rho}), \tag{7}$$

where the summation is over all reciprocal-lattice vectors, $\vec{G}_m$, of the 2D grating, and ρ is the in-plane coordinate.

The slab waveguide geometry naturally lends itself to the use of a Green's-function approach, developed by Sipe,[17] for calculating the fields generated by a planar source in the presence of a multilayer dielectric structure. In the absence of any external driving fields, for the periodic polarization potential $\vec{P}_g(\vec{r})$ of Eq. (6), the particular solution to the inhomogeneous Maxwell equations (4) is given by

$$\vec{E}(\vec{r})=\sum_m \vec{E}(\vec{\beta}+\vec{G}_m;z)\exp[i(\vec{\beta}+\vec{G}_m)\cdot\vec{\rho}], \tag{8}$$

with

$$\vec{E}(\vec{\beta};z)=\int dz'\,\vec{\vec{g}}(\vec{\beta};z,z')\cdot\sum_m \chi_{\vec{G}_m}(z')\vec{E}(\vec{\beta}-\vec{G}_m;z'). \tag{9}$$

The tensor $\vec{\vec{g}}$ is a sort of generalized Green's function that correctly takes into account all of the additional multiple reflections associated with the multilayer slab adjacent to the grating layer. To solve self-consistently for the field in the grating layer, since the Fourier components of the susceptibility $\chi_{\vec{G}_m}$ are nonzero only in the textured region, we only need the generalized Green's function over this region.[17] That is,

$$\begin{aligned}\vec{\vec{g}}(\vec{\beta};z,z')=&\vec{\vec{g}}_+(\vec{\beta})\,\theta(z-z')\exp[iw(\beta)(z-z')]\\&+\vec{\vec{g}}_-(\vec{\beta})\,\theta(z'-z)\exp[-iw(\beta)(z-z')]\\&-4\pi\delta(z-z')\hat{z}\hat{z}\\&+\vec{\vec{r}}(\vec{\beta})\cdot\vec{\vec{g}}_-(\vec{\beta})\exp[iw(\beta)(z+z')],\end{aligned} \tag{10}$$

where $\theta(z)$ and $\delta(z)$ are the Heaviside and Dirac δ functions, respectively. The first two terms in Eq. (10) are the vector analogs of the Green's function for the scalar wave equation, and describe plane waves propagating away from the polarization source in the $\pm\hat{z}$ direction with in-plane wave-vector component $\vec{\beta}$. The tensors are defined using dyadic notation as

$$\vec{\vec{g}}_\pm(\vec{\beta})=C(\beta)[\hat{s}(\vec{\beta})\hat{s}(\vec{\beta})+\hat{p}_\pm(\vec{\beta})\hat{p}_\pm(\vec{\beta})], \tag{11}$$

with the constants

$$C(\beta)=\frac{2\pi i\tilde{\omega}^2}{w(\beta)} \tag{12}$$

and

$$w(\beta)=(\tilde{\omega}^2-\beta^2)^{1/2}. \tag{13}$$

Equation (13) follows directly from the dispersion relation for plane waves in free space; $w(\beta)$ is the $\hat{z}$ component of the wave vector. The unit vectors $\hat{s}(\vec{\beta})$ and $\hat{p}_\pm(\vec{\beta})$ describe the unit s and p polarization directions, and are defined in terms of the in-plane wave vector $\vec{\beta}$ and the surface normal $\hat{z}$ as

$$\hat{s}(\vec{\beta})=\hat{\beta}\times\hat{z} \tag{14}$$

and

$$\hat{p}_\pm(\vec{\beta})=\frac{\beta\hat{z}\mp w(\beta)\hat{\beta}}{\tilde{\omega}}. \tag{15}$$

The third term in Eq. (10) describes a contribution to the electric field present only in the grating layer. It essentially describes the reduction of the polarization induced in the grating due to the $\hat{z}$ component of the electric field there. This depolarization effect can be traced to the requirement that $\nabla\cdot\vec{D}=0$ across the boundaries of the grating layer. Thus it appears in addition to the usual Green's-function terms associated with the scalar wave equation.

The fourth term in Eq. (10) describes a contribution to the electric field due to the components of the field that are downward propagating (or decaying) from the grating layer which then reflect off the multilayer slab beneath. The significant advantage of the generalized Green's-function technique is found here in that all the boundary conditions for the multilayer slab beneath the textured layer are simply contained within the reflectance tensor. It is defined as

$$\vec{\vec{r}}(\vec{\beta})=r_s(\beta)\hat{s}(\vec{\beta})\hat{s}(\vec{\beta})+r_p(\beta)\hat{p}_+(\vec{\beta})\hat{p}_-(\vec{\beta}), \tag{16}$$

in which the coefficients $r_s(\beta)$ and $r_p(\beta)$ are the Fresnel reflection coefficients for the multi-layer slab for s and p polarizations, respectively.[18] The Fresnel coefficients are, in fact, simply a restatement of all the boundary conditions for the multilayer slab and, therefore, in this formulation, any solution implicitly satisfies the boundary conditions for the entire textured slab.

To self-consistently calculate the total field in the grating, we form a system of equations involving the Fourier components of the electric field coupled together by the grating. For each reciprocal-lattice vector $\vec{G}_m$, there is an equation for the associated component of the total field, $\vec{E}(\vec{\beta}-\vec{G}_m;z)$, that has the form of Eq. (9). To simplify the notation we use a subscript to label the in-plane Fourier component of the electric field associated with the reciprocal-lattice vector $\vec{G}_m$; we write $\vec{E}_m(z)=\vec{E}(\vec{\beta}-\vec{G}_m;z)$, so that Eq. (9) becomes

$$\vec{E}_n(z)=\int dz'\,\vec{\vec{g}}_n(z,z')\cdot\sum_m \chi_{nm}(z')\vec{E}_m(z'), \tag{17}$$

where $\vec{\vec{g}}_n$ is the Green's-function tensor associated with the in-plane wave vector $\vec{\beta}_n=\vec{\beta}-\vec{G}_n$, and $\chi_{nm}(z)$ is the Fourier coefficient of the grating susceptibility coupling the mth component to the nth one. The infinite system of integral equations, of which Eq. (17) is one, is an exact representation of Maxwell's equations (4), and self-consistently determines the field in the grating layer for any slab waveguide textured periodically in the plane.

We now make some simplifying assumptions. For thin gratings in which the grating thickness is much less than the wavelength of light in the grating material, i.e., $t_g \ll 2\pi/(\tilde{\omega}\sqrt{\epsilon_g})$, the variation of the electric field in the grating, as a function of z, is small. Thus conceptually, we may replace the finite thickness grating, which acts as the spatially dependent source polarization in the inhomogeneous

Maxwell equations (4), by a δ-function grating that possesses the same effective spatially dependent polarization. This allows us to transform the system of integral equations (17) into a system of algebraic equations. First, in assuming that the variation of the electric field in the $\hat{z}$ direction in the grating is negligible, we take $\vec{E}_n(z)\approx\vec{E}_n(z_0)$, where z_0 is at the center of the grating. In addition, for a thin grating, we have $w(\beta)t_g \ll 1$ and take the phase factors in the Green's function, Eq. (10), as unity. Thus by defining the average of the grating susceptibility for each Fourier component as

$$\chi_{nm}=\frac{1}{t_g}\int_0^{t_g}\chi_{nm}(z')dz', \tag{18}$$

Eq. (17) becomes

$$\vec{E}_n(z_0)=\overleftrightarrow{g}_n\cdot\sum_m t_g\chi_{nm}\vec{E}_m(z_0). \tag{19}$$

The Green's-function tensor is now independent of z and is given by

$$\overleftrightarrow{g}_n=C_n\left[(1+r_{s_n})\hat{s}_n\hat{s}_n+\frac{\hat{p}_{n+}\hat{p}_{n+}}{2}+\frac{\hat{p}_{n-}\hat{p}_{n-}}{2}+r_{p_n}\hat{p}_{n+}\hat{p}_{n-}\right]$$
$$-\frac{4\pi}{t_g}\hat{z}\hat{z}, \tag{20}$$

where again the subscript n indicates the associated in-plane wave vector, i.e. $C_n=C(\beta_n)$, etc. Thus Eqs. (19) and (20) self-consistently determine the field in a δ-function grating layer that is approximately equivalent to the thin grating layer of Fig. 1.

In order to make the problem tractable, the summation is over only a finite number N of the lowest-order Fourier components. We reduce the N vector equations to a system of $3N$ scalar equations by projection of Eq. (19) onto the vectors $\hat{s}_n$, $\hat{\beta}_n$, and $\hat{z}$. This gives

$$E_{s_n}=\hat{s}_n\cdot\overleftrightarrow{g}_n\cdot\sum_m t_g\chi_{nm}\vec{E}_m$$
$$E_{\beta_n}=\hat{\beta}_n\cdot\overleftrightarrow{g}_n\cdot\sum_m t_g\chi_{nm}\vec{E}_m, \tag{21}$$
$$E_{z_n}=\hat{z}\cdot\overleftrightarrow{g}_n\cdot\sum_m t_g\chi_{nm}\vec{E}_m.$$

Formally, this system of equations may be written in matrix form as

$$\vec{v}=\overleftrightarrow{M}_{\vec{\beta},\tilde{\omega}}\cdot\vec{v}, \tag{22}$$

where $\vec{v}$ is a $3N\times1$ column vector comprised of the $3N$ components of the electric field in the grating, E_{s_n}, E_{β_n}, and E_{z_n}; and $\overleftrightarrow{M}$ is a $3N\times3N$ matrix parametrized by the in-plane wave vector $\vec{\beta}$ and the normalized frequency $\tilde{\omega}$. Equation (22) only has solutions for

$$\det[\overleftrightarrow{M}_{\vec{\beta},\tilde{\omega}}-\overleftrightarrow{U}]=0, \tag{23}$$

where $\overleftrightarrow{U}$ is the $3N\times3N$ identity matrix. In general, solutions to Maxwell's equations that correspond to resonant modes of a multilayer dielectric structure appear as poles in the complex $\tilde{\omega}$ plane of the reflection coefficient, for a fixed in-plane wave vector.[19] One can show that the reflection coefficient for plane waves incident on the 2D textured waveguide considered here is proportional to $[\overleftrightarrow{M}_{\vec{\beta},\tilde{\omega}}-\overleftrightarrow{U}]^{-1}$,[20] and thus poles in the reflection matrix are consistent with solutions to Eq. (23). For a given textured slab waveguide, these poles represent the allowed complex frequencies of the resonant electromagnetic excitations attached to the waveguide. By determining these complex frequencies as a function of real $\vec{\beta}$ over the first Brillouin zone, we obtain the full photonic band structure of the guided modes of the textured guide. The real and imaginary parts of the band structure describe the dispersion and lifetimes of the resonant excitations of the multilayer slab. This simple numerical procedure is completely general for thin surface gratings, and is capable of treating any 2D periodic texture by inclusion of the appropriate Fourier components.

B. Coupled-mode limit

The simplicity of the above numerical approach is appealing. However, in order to gain some physical insight into the nature of the resonant excitations of the textured slab, we further simplify Eqs. (21) in a manner analogous to the perturbative coupled mode limit.[6] From this we are able to cast our model in the form of an eigenvalue problem: the eigenvalues form the photonic band structure of the multilayer slab. This has several advantages. First, eigenvalue problems are typically computationally less intensive than pole finding in the complex plane. Second, in solving the eigenvalue problem, one obtains the photonic Bloch states directly as the corresponding eigenvectors. This gives a physical description of the resonant excitations in terms of linear combinations of modes of the untextured guide. Third, the nature of the coupling between the modes of the untextured guided is plainly revealed. In particular, we have already shown how in 1D gratings the Green's-function formalism gives physical insight into the peculiar nature of TM mode coupling due to depolarization effects in the grating.[21]

A consequence of Bloch's theorem for periodic structures is that all modes separated by a reciprocal-lattice vector $\vec{G}_m$ are equivalent. This allows the dispersion of the photonic Bloch states to be described using the reduced zone scheme. In the reduced zone scheme, those states with energies above the vacuum light line, $\tilde{\omega}=\beta$, have a radiative component, and are leaky. To illustrate the coupled-mode limit to our model, we consider coupling between guided modes near the second-order Bragg condition of a 2D texture. This is the most general situation in which there is coupling between guided modes and radiative waves, analogous to the cases we investigated previously[16] and related to the physics of resonant grating filters.[5]

The basic assumptions underlying coupled-mode theory are: first, only the modes of the untextured waveguide (TE or TM) that are nearly phased matched to the grating, need to be included in the expansion of the field; and second, the coupling between these ''dominant'' modes may be treated perturbatively. For an arbitrary 2D grating, there are N dominant guided modes near the second-order Bragg condition, and a single radiation mode, which we label $\vec{E}_0$, having polarization to be determined by the model.

For a second-order grating the radiation mode propagates nearly normal to the surface of the textured waveguide when near the zone center. We treat the coupling to this mode by first solving the textured waveguide equation (19) for $\vec{E}_0$ explicitly in terms of the N guided modes. This gives

$$\vec{E}_0 = \overleftrightarrow{h} \cdot \sum_{m=1}^{N} t_g \chi_{0m} \vec{E}_m. \tag{24}$$

The summation is over the N guided modes that are nearly phase matched to the grating, and χ_{0m} is the component of the grating susceptibility that couples the mth guided mode to the radiation mode. We have defined the tensor

$$\overleftrightarrow{h} = (1 - t_g \chi_{00} \overleftrightarrow{g}_0)^{-1} \overleftrightarrow{g}_0, \tag{25}$$

which is dependent on the normalized frequency $\tilde{\omega}$ and the in-plane wave vector $\vec{\beta}$ of the radiative component.

The in-plane and normal components of a given Fourier component of the field are not independent. By substitution of Eq. (24) into Eqs. (21), we show in the Appendix that one obtains a relationship of the form

$$\vec{E}_z = \overleftrightarrow{K}_s \cdot \vec{E}_s + \overleftrightarrow{K}_\beta \cdot \vec{E}_\beta. \tag{26}$$

Here the field components have been written as $N \times 1$ column vectors, and $\overleftrightarrow{K}_s$ and $\overleftrightarrow{K}_\beta$ are $N \times N$ matrices. Equation (26) is the textured waveguide analog to the relationship between the in-plane and normal components of the electric field in a TM mode of an untextured slab waveguide. Using this relation, we may eliminate the E_{z_n} components from our set of equations, reducing them to a system of $2N$ equations involving only the in-plane components E_{s_n} and E_{β_n} of the electric field. Note that one may have anticipated this result since, for a given wave vector, there are only two (not three) transverse solutions to Maxwell's equations.

The key approximation that allows us to cast the Green's-function formalism as an eigenvalue problem in the coupled mode limit is to keep only the resonant terms in the Green's function [Eq. (20)]. For in-plane wave vectors corresponding to a guided mode, the Fresnel reflection coefficients for the multilayer slab, r_{s_n} and r_{p_n}, are dominated by the poles at the guided mode energies $\tilde{\omega}_{s_n}$ and $\tilde{\omega}_{p_n}$ for TE and TM polarizations, respectively. Therefore, for s polarization, we approximate

$$r_{s_n} \approx \frac{R_{s_n}}{\tilde{\omega} - \tilde{\omega}_{s_n}}, \tag{27}$$

and, for p polarization,

$$r_{p_n} \approx \frac{R_{p_n}}{\tilde{\omega} - \tilde{\omega}_{p_n}}, \tag{28}$$

where R_{s_n} and R_{p_n} are the residues of the poles at the corresponding guided mode energies. [i.e., $R_{s_n} = \lim_{\tilde{\omega} \to \tilde{\omega}_{s_n}} (\tilde{\omega} - \tilde{\omega}_{s_n}) r_{s_n}$.] We keep only these resonant terms in Eq. (20), and approximate the Green's function as

$$\overleftrightarrow{g}_n \approx C_n [r_{s_n} \hat{s}_n \hat{s}_n + r_{p_n} \hat{p}_{n+} \hat{p}_{n-}] - \frac{4\pi}{t_g} \hat{z}\hat{z}. \tag{29}$$

Physically, the approximate Green's function includes only the resonant reflection from the multilayer slab due to the downward ''propagating'' component of the field radiated by the polarization induced in the grating. The $\hat{z}\hat{z}$ term takes care of the reduction in the $\hat{z}$ component of the polarization induced in the grating due to the $\hat{z}$ component of the electric field there, self-consistently. This depolarization effect was found to be important to obtain the correct form of the TM-TM coupling coefficient in 1D gratings.[21]

With these approximations, Eqs. (21) become

$$(\tilde{\omega} - \tilde{\omega}_{s_n}) E_{s_n} = C_n R_{s_n} \hat{s}_n \cdot \left(\sum_m t_g \chi_{nm} \vec{E}_m + t_g \chi_{n0} \overleftrightarrow{h} \cdot \sum_m t_g \chi_{0m} \vec{E}_m \right),$$

$$(\tilde{\omega} - \tilde{\omega}_{p_n}) E_{\beta_n} = C_n R_{p_n} (\hat{\beta}_n \cdot \hat{p}_{n+}) \hat{p}_{n-} \cdot \left(\sum_m t_g \chi_{nm} \vec{E}_m + t_g \chi_{n0} \overleftrightarrow{h} \cdot \sum_m t_g \chi_{0m} \vec{E}_m \right). \tag{30}$$

Equations (30) give a self-consistent calculation of the modes of the textured waveguide, within the resonant pole approximation.

We now drop the self-consistency and derive an eigenvalue problem in $\tilde{\omega}$. We identify the $\hat{s}_n$ component of the field with the nth TE mode, and the $\hat{\beta}_n$ component with the nth TM mode and consider these as basis states for an expansion of the photonic eigenstates of the textured waveguide. Note that the polarization unit vectors $\hat{p}_{n+}$ and $\hat{p}_{n-}$, the coupling to the radiative component, $\overleftrightarrow{h}$, the renormalization matrices $\overleftrightarrow{K}_s$ and $\overleftrightarrow{K}_\beta$, and the constants C_n on the right hand side of Eq. (30) rigorously depend on $\tilde{\omega}$. In the spirit of a perturbative approach, to evaluate these parameters we assume that they take on their values at the appropriate unperturbed mode energy $\tilde{\omega}_{s_n}$ or $\tilde{\omega}_{p_n}$ for TE or TM modes, respectively. This leads to an eigensystem that may be written in matrix form as

$$\overleftrightarrow{M}_{\vec{\beta}} \cdot \vec{u} = \tilde{\omega} \vec{u}, \tag{31}$$

where the matrix elements are given by

$$m_{s_n s_m} = \delta_{nm} \tilde{\omega}_{s_n} + C_n R_{s_n} [t_g \chi_{nm} (\hat{s}_n \cdot \hat{s}_m) + t_g^2 \chi_{n0} \chi_{0m} h_{s_n s_m}], \tag{32}$$

$$m_{s_n \beta_m} = C_n R_{s_n} [t_g \chi_{nm} (\hat{s}_n \cdot \hat{\beta}_m) + t_g^2 \chi_{n0} \chi_{0m} h_{s_n \beta_m}], \tag{33}$$

and

$$m_{\beta_n\beta_m}=\delta_{nm}\tilde{\omega}_{\beta_n}+C_nR_{p_n}(\hat{\beta}_n\cdot\hat{p}_{n+})t_g\chi_{nm}\times\left[(\hat{p}_{n-}\cdot\hat{\beta}_m)+(\hat{p}_{n-}\cdot\hat{z})\sum_{k=1}^{N}t_g\chi_{nk}(K_\beta)_{km}\right]+C_nRp_n\beta_nt_g\chi_{n0}\left[t_g\chi_{0m}h_{p_{n-}\beta_m}+h_{p_{n-}z}\sum_{k=1}^{N}t_g\chi_{0k}(K_\beta)_{km}\right], \quad (34)$$

$$m_{\beta_ns_m}=C_nRp_n(\hat{\beta}_n\cdot\hat{p}_{n+})t_g\chi_{nm}\times\left[(\hat{p}_{n-}\cdot\hat{s}_m)+(\hat{p}_{n-}\cdot\hat{z})\sum_{k=1}^{N}t_g\chi_{nk}(K_s)_{km}\right]+C_nRp_n\beta_nt_g\chi_{n0}\left[t_g\chi_{0m}h_{p_{n-}s_m}+h_{p_{n-}z}\sum_{k=1}^{N}t_g\chi_{0k}(K_s)_{km}\right], \quad (35)$$

where, for example, we have used the notation, $h_{p_{n-}s_m}=\hat{p}_{n-}\cdot\overleftrightarrow{h}\cdot\hat{s}_m$.

The elements of the coupled-mode matrix, $\overleftrightarrow{M}_{\vec{\beta}}$, have simple physical interpretations. The diagonal elements $m_{s_ns_n}$ and $m_{\beta_n\beta_n}$ describe the change in the energy of a TE or TM mode, respectively, due to the additional material in the textured guide associated with the grating. This effect is proportional to χ_{nn} which is the average or dc component of the susceptibility in the grating region. As more material is added, the energy of a mode is reduced. The self-energy is also changed due to the second order (in t_g) coupling via the radiative component. The off-diagonal terms $m_{s_ns_m}$ describe the direct coupling between the nth and mth TE basis states, or modes of the untextured guide. The coupling coefficient κ used in conventional coupled mode theory is proportional to this matrix element. The first-order contribution is proportional to the Fourier component of the grating χ_{nm}, which causes the basis states to be phase matched, and the dot product of the unit vectors associated with the electric field of the mode. In the usual 1D case, this dot product is -1, but in two dimensions, TE mode coupling depends strongly on the direction of propagation in the plane. In fact, TE modes propagating perpendicularly to each other in the plane do not couple together to first order. The second-order contribution in the off-diagonal terms is due to coupling to the radiating wave and to coupling from the radiating wave back into the guided mode; the effect is proportional to the appropriate matrix element of the radiative tensor $\overleftrightarrow{h}$. This matrix element is in general complex, and thus coupling to radiative waves is described in conventional coupled-mode theory using a complex coupling coefficient κ.[7] In a similar manner, the coupling between the nth TE mode and the mth TM mode is described by a combination of the matrix element $m_{s_n\beta_m}$ and $m_{\beta_ms_n}$. The coupling between the TM modes themselves, described by the matrix elements $m_{\beta_m\beta_n}$, is qualitatively different than that between TE modes. The $\hat{z}$ component of the TM modes provides additional coupling which is described through the sum over the matrix $\overleftrightarrow{K}_\beta$ between them. Since the TM-like components of the field are now described solely by their in-plane component, the normal component coupling appears effectively as a renormalization of the in-plane coupling through the matrices $\overleftrightarrow{K}_s$ and $\overleftrightarrow{K}_\beta$.

This completes the derivation of a simple, heuristic, 2D vector model that describes coupling in waveguides that have been textured with a thin 2D surface grating. The TE and TM modes of the untextured guide are considered as basis states of the eigenvalue problem, [Eq. (31)]. The complex eigenfrequencies describe the dispersion and lifetimes of the photonic eigenstates of the textured slab, and the eigenvectors describe the eigenstates themselves. In Sec. III, we solve this model in the case of leaky mode coupling and bound mode coupling.

III. ILLUSTRATIVE EXAMPLES

In this section we use the coupled-mode formalism described above to illustrate various distinguishing features in the photonic band structure of resonant modes in 2D textured, planar waveguides. One-dimensional texture typically couples two nearly degenerate slab modes that have in-plane wave vectors approximately equal to half of one of the reciprocal-lattice vectors of the grating. If the modes propagate parallel to the grating wave vector, the coupling can only occur between TE modes or between TM modes; there is no TE-TM coupling. This is the usual situation encountered in DFB lasers, and grating filters. However, if the slab modes are obliquely incident on a 1D grating, it is possible to couple TE and TM modes (as long as the components of the wave vectors in the grating direction, for both modes, are nearly equal to half of one of the reciprocal-lattice vectors of the grating). Already for the oblique incidence case in one dimension, the vector nature of the coupling problem introduces subtle but very important effects due to depolarization of the $\hat{z}$ component of the modes (associated with the $\hat{z}\hat{z}$ term in $\overleftrightarrow{g}$).[21] Although the concept of a photonic band structure is valid, and is sometimes used to describe 1D textured structures, it provides little additional insight.

The coupling introduced by 2D texture is far richer: the importance of depolarization fields remains, while the flexibility of having five distinct Bravais lattices substantially increases the number of modes that can be coupled to one another. By judicious choice of the slab mode dispersion, the grating symmetry, and the lattice constant, it is possible to couple TE (TM) modes with other TE (TM) modes, or with TM (TE) modes, at virtually any point in the first Brillouin zone. The relevant modes may or may not propagate along the same direction in the plane. The photonic band-structure interpretation of the coupled modes in two dimensions does offer significant advantages in understanding these complexities. For instance, the labels TE and TM cannot be rigorously applied to the resonant eigenstates of 2D textured waveguides: all eigenstates contain some admixture of both TE and TM modes. However, we show below that it is possible to label each photonic band with a well-defined polarization that is associated with the Fourier component of the eigenstate that lies within the first Brillouin zone. When the eigenmode exists above the light line, this lowest order Fourier component actually radiates into the surrounding vacuum, rendering the state leaky, and giving it a finite lifetime. The band structure is therefore inherently complex. However, there are important symmetries associated with the imaginary part of the band structure which can lead to eigenstates that exist above the light line having infinite lifetimes. Thus, in special cases, bound states can still exist above the light line in 2D textured waveguides.

These properties, the inherent vector nature of the photonic eigenstates and their manifestly complex band structure, are fundamental differences between 2D textured waveguides and 2D photonic crystals composed of infinitely long dielectric cylinders or holes in a dielectric block. The following provides explicit examples of band structures, both real and imaginary, calculated using the formalism developed in this paper that illustrate these fundamental differences. All examples use a 2D square lattice because it is the simplest nontrivial symmetry that illustrates most of the effects alluded to above.

A. Leaky mode coupling

We begin by studying the coupling of TE and TM slab modes with wave vectors in the vicinity of the smallest four reciprocal-lattice vectors of a square lattice (eight modes in all). The corresponding eigenstates represent the eight lowest-energy modes near the Brillouin zone center in the reduced zone scheme. Since all of these eigenstates exist above the vacuum light line, they are all in general leaky, and it is the polarization of the leaky component of each mode that represents a ''good quantum number.''

Maxwell's equations scale as ω/L, where L is some length scale.[10] For a textured waveguide, we choose the length scale to be the lattice constant Λ of the 2D texture. For simplicity, we consider a single-layer dielectric waveguide of thickness $t_s/\Lambda=1.0$, having a dielectric constant $\epsilon_s=12.25$, above which is a grating of thickness $t_g/\Lambda=0.1$, that has been textured in two dimensions with a regular square lattice, with period Λ, of air holes. The diameter of the holes is such that the air-filling fraction in the grating layer is 0.5. The reciprocal-lattice vectors of the grating may be written as

$$\vec{G}=j\beta_g\hat{x}+k\beta_g\hat{y} \tag{36}$$

for all integers j and k, where we have defined the grating wave vector $\beta_g=2\pi/\Lambda$. For a 2D square lattice grating, near the second-order Bragg condition, there are four dominant guided modes with $\vec{\beta}\approx\{\pm\beta_g,0\}$ and $\{0,\pm\beta_g\}$ for each polarization. Thus, to capture the basic physics involved, we include eight guided modes (four TE and four TM) and one radiation mode in our coupled-mode formalism.

To determine the band structure, we first calculate the parameters that depend only on properties of the untextured waveguide. The effective indices n_e^{TE} and n_e^{TM} for the guided modes of the untextured guide at the second-order Bragg condition are determined simply by solving the planar waveguide problem at $\beta=\beta_g$. The normalized energy of the TE guided mode so calculated, $\tilde{\omega}_{s_0}$, is used to determine the effective index through the relation $n_e^{TE}=\beta/\tilde{\omega}_{s_0}$. The variation in the unperturbed mode energy of the nth TE mode is approximated as a function of in-plane wave vector as

$$\tilde{\omega}_{s_n}\approx\frac{\beta_g}{n_e}+\frac{|\vec{\beta}_n-\vec{\beta}_g|}{n_g}, \tag{37}$$

where n_e is the TE effective index, and

$$n_g=n_e+\beta(dn_e/d\beta) \tag{38}$$

is the group effective index of the TE guided mode. An analogous calculation is performed for the TM guided modes. This approximation serves to limit the number of times that the untextured waveguide problem must be solved. However, the extent to which the dispersion of the guided modes of the untextured guide is accurately described by Eq. (37) limits the range in wave vectors that this form of the model is applicable. Finally, the residues R_s and R_p are calculated from the well-known reflection coefficients for a multilayer slabs using Fresnel coefficients.[18]

The parameters associated with the 2D textured layer are also needed. The linear susceptibility of the grating is related to the dielectric function of the grating layer, $\epsilon_g(\vec{r})=1+4\pi\chi_g(\vec{r})$. We calculate the Fourier coefficients χ_{nm} of the linear susceptibility using the inverse of Eq. (7) and then average over the grating layer using Eq. (18).

With these parameters, we then solve the eigenvalue problem [Eq. (31)], as a function of the in-plane wave vector. The real part of the eigenstate frequency is plotted in Fig. 2 versus the in-plane propagation constant β as it is detuned away from the second-order Bragg condition in the X (1-0) direction on the right half of the figure, and the M (1-1) direction on the left half. The general form of the band structure can be understood simply in terms of zone folding the guided mode dispersion of the untextured guide into the first Brillouin zone using square lattice symmetry. However, in regions where zone folding leads to overlapping bands, the degeneracy is split, and where zone folding gives band crossings, anticrossings can appear due to the coupling induced by the grating. Unlike infinite 2D photonic crystals, these anticrossings can occur between bands associated principally with TE and TM modes. The anticrossings appear at the zone boundaries, as usual, but also may appear away from zone boundaries as discussed below.

At the zone center there are two ''gaps,'' each characterized by four bands anticrossing. The higher-energy gap corresponds to perturbed TM slab modes, and the lower-energy one corresponds to the perturbed TE slab modes. The energy separation between these two gaps occurs because the effective index for TM slab modes is lower than that for TE slab modes in an untextured guide. We now focus our attention on the character of the photonic eigenstates near the band edges of the TM gap, shown on an expanded scale in Fig. 3.

The highest-energy states near the band-edge state of the TM gap consist primarily of an in-phase superposition of all four TM modes traveling in the $\{\pm\beta_g,0\}$ and $\{0,\pm\beta_g\}$ directions, [i.e., with eigenvector $\propto$ (1,1,1,1)]. Thus the photonic modes are essentially 2D standing waves, and in the grat-

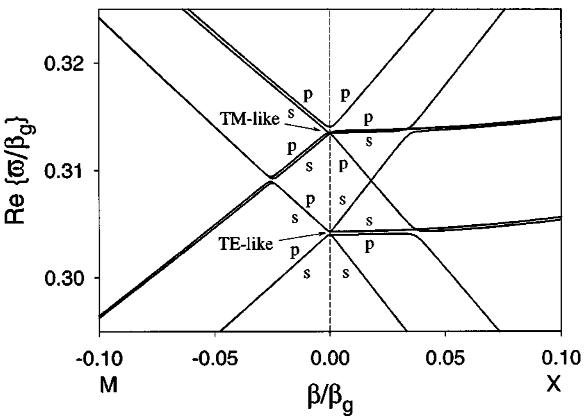

FIG. 2. Real part of the photonic band structure for a 2D square lattice texture illustrating the dispersion of photonic eigenstates near the zone center as the in-plane wave vector is detuned in the X (1-0) symmetry direction on the right half and the M (1-1) symmetry direction on the left half. The band-edge states near the higher-energy ''gap'' are TM-like states; the lower-energy ones are TE-like. The polarization of the radiative component (s or p) associated with each band is also indicated. The structure contains a square lattice of air holes with filling fraction 0.5, with $t_g/\Lambda=0.1$ and $t_s/\Lambda=1.0$.

ing layer, the mode intensity is greatest in the air holes of the 2D lattice. The lowest-energy states in the vicinity of the band edge consist mainly of in-phase superpositions of the forward- and backward-traveling TM modes in the $\hat{x}$ direction, out of phase with those traveling in the $\hat{y}$ direction, [i.e., (1,1,−1,−1)]. The middle band-edge eigenstates of the TM gap, in this case, are degenerate in energy. These two states consist primarily of in-phase superpositions of forward- and backward-traveling TM slab modes in the $\hat{x}$ direction, and antiphase superpositions in the $\hat{y}$ direction and vice versa. [i.e., (1,1,1,−1) and (1,−1,1,1,)]. This symmetry, the existence of two degenerate and two nondegenerate states at the zone center, is a fundamental property of a square lattice of circular holes.[22]

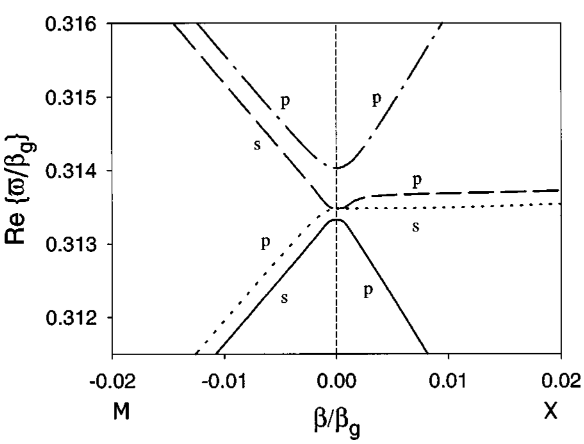

FIG. 3. Expanded scale view of Fig. 2 near the TM gap showing the fundamental symmetry of the band-edge states at the zone center for a square lattice of circular holes. The in-plane wave vector is detuned in the X (1-0) symmetry direction on the right half, and in the M (1-1) symmetry direction on the left half. Various line types are used to indicate correspondence with the imaginary part of the band structure shown in Fig. 4.

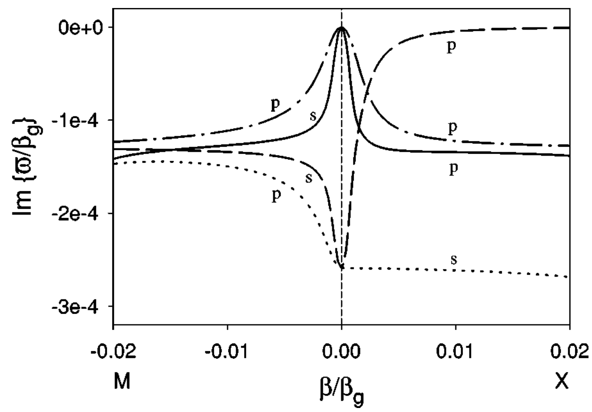

FIG. 4. Imaginary part of the photonic band structure for a 2D square lattice texture illustrating the decay rates of the TM-like photonic eigenstates shown in Fig. 3. The in-plane wave vector is detuned in the X (1-0) symmetry direction on the right half, and in the M (1-1) symmetry direction on the left half. The TE-like photonic eigenstates (not shown) are qualitatively the same. The line types used indicate the corresponding real part in Fig. 3.

Unique to the waveguide geometry, the first-order Fourier components of the 2D grating couple the slab modes propagating in the plane of the guide to a radiative component propagating nearly normal to the surface of the guide. Since all of the eigenstates shown in Fig. 2 are above the vacuum light line, $\tilde{\omega}=\beta$, they are expected to be leaky. The leakiness of photonic eigenstates is described in terms of the imaginary part of the eigenstate frequency, $\tilde{\omega}^i$. The lifetime of an eigenstate is inversely proportional to $\tilde{\omega}^i$; for $\tilde{\omega}^i=0$ the eigenstates are not lossy, and have infinite lifetimes. Figure 4 shows $\tilde{\omega}^i$ versus β, corresponding to the four bands emanating from the TM-like gap shown in Fig. 3. At the zone center, the highest- and lowest-energy band-edge eigenstates have infinite lifetimes and are not leaky but true bound excitations of the texture slab waveguide. Since these eigenstates are in-phase superpositions of the forward- and backward-propagating slab modes described above, the resulting radiative components add destructively. (Recall that due to the vector nature of the problem, forward- and backward-traveling modes have their in-plane electric-field vectors in opposite directions. Thus an in-phase superposition is one of destructive interference.) The degenerate band edge states are lossy for the converse reason.

As the propagation constant is detuned from the zone center (second-order Bragg condition), all of the eigenstates become lossy regardless of the direction in the plane of the detuning. Clearly some of the states, those with $\tilde{\omega}^i$ small, are tightly bound to the slab waveguide, whereas others are relatively weakly bound. These lossy eigenstates are analogous to Fano resonances; the texture couples the discrete slab modes of the untextured guide to the radiation mode continuum, and the imaginary part of the eigenfrequency reflects the strength of this coupling. Thus one may expect that probing these states via their radiative components will result in a sharp, narrow resonance for $\tilde{\omega}^i$ small, and a broad resonance for the weakly bound states.[23] The existence of the degenerate and lossy band-edge states is the basis for polarization-

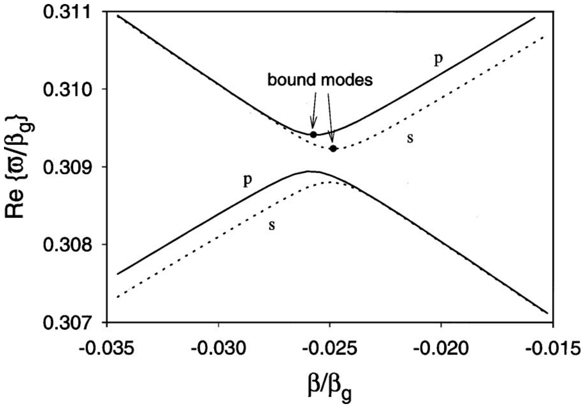

FIG. 5. Real part of the photonic band structure near the anticrossing between TE-like and TM-like bands.

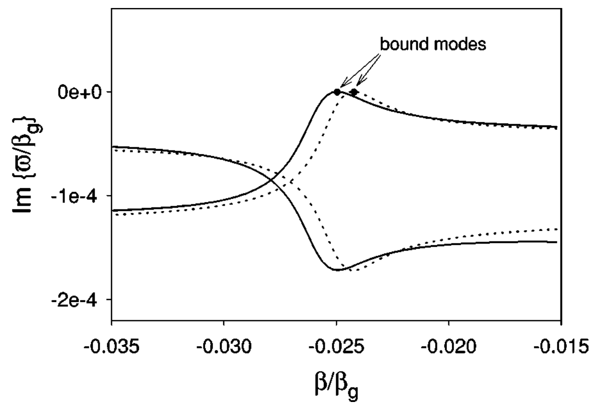

FIG. 6. Imaginary part of the photonic band structure corresponding to Fig. 5. Note that $\tilde{\omega}^i$ goes to zero for the higher-energy band-edge states near the anticrossing, indicating a truly bound eigenstate.

insensitive resonant grating filters; the degeneracy allows the state to be excited by a plane wave with any incident polarization.

A calculation of the eigenvectors associated with a particular photonic band shows that the eigenstates are neither purely TE nor purely TM in character. However, the polarization of the radiative component of a particular photonic band, calculated via Eq. (24), is well defined as indicated on Fig. 2. For an arbitrary detuning direction, the polarization of the radiative component of a particular eigenstate near the second-order gap is elliptical with an orientation dependent on the detuning direction. In general, however, for detuning along axes possessing reflection symmetry (such as X or M), the polarization of the radiation is always either s or p. Thus, for leaky eigenstates, the polarization of the zeroth-order Fourier component of the polarization in the grating is an appropriate label for identifying the photonic bands.

A remarkable feature of the 2D band structure of the photonic eigenstates in the planar waveguide geometry, which does not occur for plane-wave propagation (in the plane of the periodicity) of infinite 2D photonic crystals studied previously by other others,[10] is the occurrence of anticrossings between TE- and TM-like eigenstates. For example, when the propagation constant is detuned from the zone center in the M direction (left half of Fig. 2), the upper bands associated with the TE gap become phase matched with the lower bands associated with the TM gap; anticrossings occur near $\beta/\beta_g \approx -0.025$. Figure 5 shows this region on an expanded scale. There are two separate anticrossings here associated with two nearly degenerate bands having orthogonal radiative components. The bands with the same polarization of the radiative component anticross. For one anticrossing, the lower-energy band-edge eigenstate is predominantly an out-of-phase superposition of the backward-propagating TE slab modes and forward-propagating TM slab modes, and the upper-energy state is predominantly the corresponding in-phase superposition. Interestingly, the coupling strength here between TE and TM slab modes is as large as TE-TE or TM-TM coupling at the zone center, as indicated by the width of the gaps, due to the shared radiative component. Figure 6 shows the imaginary part of the band structure corresponding to the four bands near this anticrossing. Here, away from zone center, phase cancellation results in one of the band-edge eigenstates being a true bound mode of the system, indicated by the imaginary part of the eigenfrequency going to zero, even though it exists above the vacuum light line. In other words, the vector nature of the coupling in 2D textured waveguides introduces additional symmetries not found in plane wave propagation in infinite 2D photonic crystals.

The coupling between the slab modes themselves at the second-order gap is primarily facilitated by the second-order Fourier components of the dielectric function describing the 2D grating. Thus the details of the symmetry of the band-edge states depend on the relative amplitudes of these components which in turn depend on the air-filling fraction of the holes forming the texture. The main effect of changing the relative amplitude of the Fourier components is to change the ordering of the degenerate and nondegenerate states. A consequence of this is that the locations of the anticrossings described above are also modified, leading to an additional variation in the behavior of the dispersion away from the zone center.

Another way of modifying the symmetry of the band-edge states is to change the strength of the texture. By changing the depth of the grating, one leaves the relative strength of the Fourier components the same but changes the overall strength of the coupling between the modes. As the coupling strength is increased, the width of both the TE and TM gaps increase. Then, in the case of very strong coupling, the TE and TM gaps would eventually become so wide that they would overlap. There would be considerable mixing between the TE and TM components of the eigenstates at the zone center, making it meaningless to denote the photonic Bloch states as predominantly TE- or TM-like. However, in this limit the thin grating approximation breaks down, and one must use more complicated modelling techniques to describe structures which have holes that penetrate through the slab.[16]

B. Bound mode coupling

In this section, we consider another application of 2D gratings in planar waveguides, illustrating coupling between bound TE modes and bound TM modes. This is achieved by designing an untextured waveguide such that TE and TM modes with wave vectors separated by a reciprocal-lattice vector of the 2D grating are nearly degenerate in energy, and

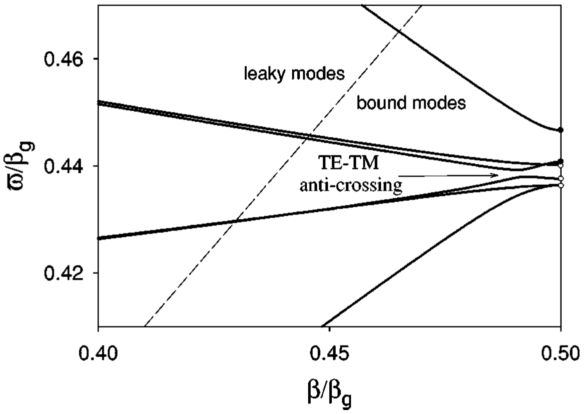

FIG. 7. Real part of the photonic band structure for a 2D square lattice texture illustrating the dispersion of photonic eigenstates near the zone boundary ($\beta=\beta_g/2$). The upper two band-edge states (solid circles) are TM-like states; the four lower-energy ones are predominantly TE-like states (open circles). The structure is a square lattice of holes with filling fraction 0.35, with $t_s/\Lambda=0.22$ and $t_g/\Lambda=0.022$.

are below the light line in the reduced zone scheme. The coupling between the modes appears in the band structure as an anticrossing between the photonic bands associated with bound TE modes and bound TM modes.

Consider a slab of thickness $t_s/\Lambda=0.22$, and a 2D grating of thickness $t_g/\Lambda=0.022$ with holes of diameter such that the air-filling fraction in the grating layer is 0.35. For this structure the resonant coupling occurs between TE modes at $\{\pm\beta_g/2,\pm\beta_g\}$ and TM modes at $\{\pm\beta_g/2,0\}$. Since these modes exist below the vacuum light line, there is no radiative component to include. This may be treated simply within our model by setting $\vec{\vec{h}}=0$. Also note that the TE modes are not traveling in the same direction in the plane as the TM modes, suggesting a possible application of this structure as a TE-TM mode converter.

To determine the photonic bandstructure, we include 12 modes (six TE and six TM at the resonant wave vectors listed above) in the model and determine the properties of the untextured guide, n_e^{TE}, n_g^{TE}, R_s, etc., for these modes. Figure 7 shows the results of solving the eigenvalue equation (31) as the in-plane wave vector is detuned from the first-order Bragg condition $\vec{\beta}=(\beta_g/2)\hat{x}$ toward the zone center. The eigenfrequencies are all purely real, indicating that these photonic eigenstates are all bound to the slab with infinite lifetimes.

One sees that there are six band-edge states below the (dashed) light line: the upper two eigenstates (solid dots) are primarily associated with the TM-like gap due to out-of-phase (highest energy) and in-phase (second highest energy) superpositions of the TM basis states at $\{\pm\beta_g/2,0\}$. The lower four eigenstates (open circles) are associated with superpositions of mostly the TE basis states at $\{\pm\beta_g/2,\pm\beta_g\}$.

The band structure of Fig. 7 shows that significant coupling may occur between the TE and TM basis states directly, even in the absence of a radiative component. At $\beta\approx-0.01\beta_g$ from the zone boundary, there is an anticrossing between a band representing the forward-traveling $\{\beta_g,0\}$ TM mode and a band representing mainly a superposition of the $\{-\beta_g/2,\beta_g\}$ and $\{-\beta_g/2,-\beta_g\}$ TE modes of the untextured guide. The coupling between TE and TM basis states occurs because, in two dimensions, the electric-field vectors of modes not traveling parallel (or antiparallel) share common in-plane components in the grating. Again we note that, in contrast, TE and TM plane waves traveling in the plane of the periodicity of infinite 2D photonic crystals, do not couple together.[10] Thus the nature of the coupling in the textured waveguides is fundamentally different from that in infinite 2D photonic crystals, due to the lack of translational symmetry in the z direction.

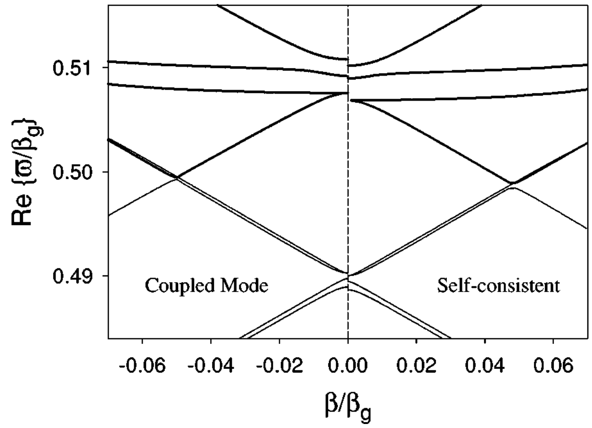

FIG. 8. Comparison of the real part of the photonic band structure near the zone center using the coupled-mode formulation (left) and the self-consistent formulation (right). The structure is a square lattice of holes with filling fraction 0.75, with $t_s/\Lambda=0.3$ and $t_g/\Lambda=0.03$.

C. Comparison with self-consistent formulation

In order to illustrate the validity of the eigenvalue formulation, in this last section we compare the band structure calculated using the 2D coupled-mode approach [Eq. (31)], with that solving the self-consistent formulation [Eq. (23)]. We consider the general case that TE and TM slab modes, not traveling in the same direction, couple together above the light line.

Again, we consider a single-layer dielectric waveguide having a dielectric constant $\epsilon_s=12.25$ that has been textured in two dimensions with a regular square lattice of air holes, with period Λ and thickness $t_g/\Lambda=0.03$. The diameter of the holes is such that the air-filling fraction in the grating layer is 0.75. For a slab of thickness is $t_s/\Lambda=0.3$, dispersion of the guided modes is such that the TE modes at $\{\pm\beta_g,\pm\beta_g\}$ and the TM modes at $\{\pm\beta_g,0\}$ and $\{0,\pm\beta_g\}$ are nearly degenerate in energy. Therefore these modes will resonantly couple near the zone center.

Figure 8 shows a comparison of the photonic eigenstate dispersion as calculated by the self-consistent theory, [Eq. (23)] on the right, and the coupled-mode limit [Eq. (31)] on the left. Figure 9 shows a similar comparison of the imaginary part of the eigenfrequency. Qualitatively the agreement is quite good as seen in both figures. In Fig. 8, the four upper band-edge photonic eigenstates are TM-like, shown with thick lines, and the lower ones are TE-like, shown with thin lines. The self-consistent theory and the coupled-mode limit both predict the width of the gaps to be effectively the same,

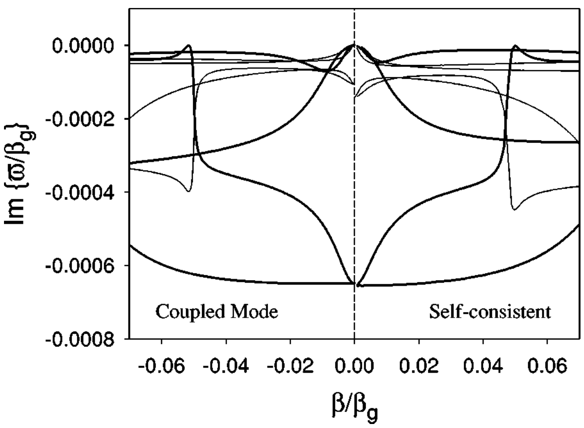

FIG. 9. Comparison of the imaginary part of the photonic band structure for the TM-like eigenstates shown in Fig. 9 using the coupled-mode formulation (left) and the self-consistent formulation (right). The thick (thin) lines correspond to bands emanating from the TM-like (TE-like) gap.

and give the same ordering of the eigenstate degeneracy. The major difference is a quantitative one due to the difference in calculating the self-energy term of a mode approximately in the coupled-mode limit. Thus the center frequency of the gaps is slightly off in the coupled-mode case, but only by less than $\sim 0.1\%$ for both TE and TM. The quantitative discrepancy is somewhat more severe for the imaginary part of the eigenfrequency, as shown in Fig. 9, about 20% in the worst case. This is good agreement considering that the grating is 1/10 the thickness of the slab.

Finally, the coupled-mode formulation is a perturbative calculation, and so is restricted in the range of wave vectors that may be considered due to approximation (37). We have shown how it may be used to calculate the dispersion near the zone center or, as in Sec. III B near a zone boundary. The advantage of the self-consistent formulation is that it may be used to calculate the band structure throughout the first Brillouin zone. The penalty one pays for this is simply one of computation time.

IV. CONCLUSION

The 2D vector coupled-mode theory developed in this paper gives considerable insight into the nature of coupling between guided modes in planar dielectric waveguides that have been textured in two dimensions with a thin surface grating. The photonic eigenstates of such structures may be thought of as linear superpositions of modes of the untextured guide. The phase relationship between the components forming the eigenstates determines many of the interesting properties of the textured waveguide, including the polarization properties and the lifetimes of the leaky eigenstates. The polarization of the radiative component turns out to be a good quantum number for labeling the photonic bands associated with leaky eigenstates.

There are two fundamental differences between 2D textured waveguides and infinite 2D photonic crystals, both due to the lack of translational invariance normal to the plane of the texture. First, the photonic eigenstates may contain a radiative component, and thus have a finite lifetime. This manifests itself in the eigenfrequencies of the photonic states being complex. Second, unlike plane waves traveling in the plane of infinite 2D photonic crystals, TE modes can couple to TM modes in 2D textured waveguides.

We illustrated, with three different examples, that the set of modes of the untextured guide that become coupled together may be controlled by judicious choice of structural parameters. TE modes couple to TE and/or TM modes, as long as the modes are nearly degenerate in energy, and a reciprocal-lattice vector of the grating separates their wave vectors. This occurs for both bound and leaky photonic eigenstates. More generally, although not explicitly shown here, first-order guided modes may be coupled to higher-order guided modes using 2D gratings when the above condition is satisfied.

Finally we note that although we have restricted the discussion to a square lattice of circular holes for pedagogical reasons, our model may be used to calculate similar properties for any 2D lattice type. It remains to be seen experimentally[24] to what extent the coupled-mode limit quantitatively applies to the dispersion and lifetimes of the resonant excitations for photonic band-gap structures in waveguide geometries.

ACKNOWLEDGMENTS

This research was supported by the Natural Sciences and Engineering Research Council of Canada and the Canadian Cable Labs Fund.

APPENDIX

In this appendix we derive the relationship between the in-plane and normal components of the electric field in a textured waveguide. We start by writing Eq. (20) as

$$\overleftrightarrow{g}_n = \overleftrightarrow{g}'_n - 4\pi/t_g \hat{z}\hat{z}, \tag{A1}$$

and substitute this into Eq. (19) which gives,

$$\vec{E}_n + 4\pi\hat{z}\hat{z}\cdot\sum_{m=0}^{N}\chi_{nm}\vec{E}_m = \overleftrightarrow{g}'_n\cdot\sum_{m=0}^{N} t_g\chi_{nm}\vec{E}_m . \tag{A2}$$

Now substituting in the expression for the radiative component gives

$$\begin{aligned}\vec{E}_n + 4\pi\hat{z}\hat{z}\cdot\left(\sum_{m=1}^{N}\chi_{nm}\vec{E}_m + \chi_{n0}\overleftrightarrow{h}\cdot\sum_{m=1}^{N} t_g\chi_{0m}\vec{E}_m\right)\\ = t_g\overleftrightarrow{g}'_n\cdot\left(\sum_{m=1}^{N}\chi_{nm}\vec{E}_m + \chi_{n0}\overleftrightarrow{h}\cdot\sum_{m=1}^{N} t_g\chi_{0m}\vec{E}_m\right).\end{aligned} \tag{A3}$$

Using the expression for the green's function [Eq. (20)], the $\hat{z}$ component of this equation can be written as

$$E_{z_n}+(4\pi-2\pi i t_g\beta_n^2/w_n)\hat{z}\cdot\left(\sum_m \chi_{nm}\vec{E}_m + \chi_{n0}\overleftrightarrow{h}\cdot\sum_m t_g\chi_{0m}\vec{E}_m\right) = r_{p_n}t_g\beta_n/\tilde{\omega}\hat{p}_{n-}\cdot\left(\sum_m \chi_{nm}\vec{E}_m+\chi_{n0}\overleftrightarrow{h}\cdot\sum_m t_g\chi_{0m}\vec{E}_m\right), \tag{A4}$$

while the $\hat{\beta}_n$ component is

$$E_{\beta_n}-2\pi i t_g w_n\hat{\beta}_n\cdot\left(\sum_m \chi_{nm}\vec{E}_m+\chi_{n0}\overleftrightarrow{h}\cdot\sum_m t_g\chi_{0m}\vec{E}_m\right) = -r_{p_n}t_g w_n/\tilde{\omega}\hat{p}_{n-}\cdot\left(\sum_m \chi_{nm}\vec{E}_m+\chi_{n0}\overleftrightarrow{h}\cdot\sum_m t_g\chi_{0m}\vec{E}_m\right). \tag{A5}$$

The right-hand sides of these two equations are proportional to within a constant factor, and thus

$$E_{z_n}+(4\pi-2\pi i t_g\beta_n^2/w_n)\hat{z}\cdot\left(\sum_m \chi_{nm}\vec{E}_m + \chi_{n0}\overleftrightarrow{h}\cdot\sum_m t_g\chi_{0m}\vec{E}_m\right) = -\beta_n/w_n E_{\beta_n} + 2\pi i t_g\beta_n\hat{\beta}_n\cdot\left(\sum_m \chi_{nm}\vec{E}_m+\chi_{n0}\overleftrightarrow{h}\cdot\sum_m t_g\chi_{0m}\vec{E}_m\right) \tag{A6}$$

There are N of these equations, one for each Fourier component, which can be written in matrix form as

$$\overleftrightarrow{M}_z\cdot\vec{E}_z=\overleftrightarrow{M}_s\cdot\vec{E}_s+\overleftrightarrow{M}_\beta\cdot\vec{E}_\beta. \tag{A7}$$

where the field components have been written as an $N\times 1$ column vector, and $\overleftrightarrow{M}_z$, $\overleftrightarrow{M}_s$, and $\overleftrightarrow{M}_\beta$ are $N\times N$ matrices. Equation (A7) may be rewritten as an explicit expression for the $\hat{z}$ components in terms of the in-plane $\hat{s}$ and $\hat{\beta}$ components:

$$\vec{E}_z=\overleftrightarrow{M}_z^{-1}\overleftrightarrow{M}_s\cdot\vec{E}_s+\overleftrightarrow{M}_z^{-1}\overleftrightarrow{M}_\beta\cdot\vec{E}_\beta=\overleftrightarrow{K}_s\cdot\vec{E}_s+\overleftrightarrow{K}_\beta\cdot\vec{E}_\beta. \tag{A8}$$

One may have anticipated this result since, for a given wave vector, there are only two (not three) transverse solutions to Maxwell's equations.

The matrix elements are found to be

$$(M_z)_{ij}=\delta_{ij}+A_i\chi_{ij}+t_g\chi_{i0}\chi_{0j}(A_ih_{zz}-B_ih_{\beta_iz}), \tag{A9}$$

$$(M_s)_{ij}=-t_g\chi_{i0}\chi_{0j}(A_ih_{zs_j}-B_ih_{\beta_is_j}), \tag{A10}$$

$$(M_\beta)_{ij}=-\beta_i/w_i\delta_{ij}+B_i\chi_{ij}-t_g\chi_{i0}\chi_{0j}(A_ih_{z\beta_j}-B_ih_{\beta_i\beta_j}), \tag{A11}$$

where

$$A_i=4\pi-2\pi i t_g\beta_i^2/w_i, \tag{A12}$$

$$B_i=2\pi i t_g\beta_i. \tag{A13}$$

Finally we note that if there is no radiative component to the field then the matrix M_s is zero, and only the $\hat{\beta}_n$ components are related to the $\hat{z}$ components of the field.

[1] S. Peng and G. M. Morris, J. Opt. Soc. Am. A **13**, 993 (1996).
[2] S. S. Wang and R. Magnusson, Appl. Opt. **32**, 2606 (1993).
[3] T. Tamir and S. Zhang, J. Opt. Soc. Am. A **14**, 1607 (1997).
[4] S. M. Norton, G. M. Morris, and T. Erdogan, J. Opt. Soc. Am. A **15**, 464 (1998).
[5] S. Peng and G. M. Morris, Proc. SPIE **2689**, 90 (1996).
[6] A. Yariv, IEEE J. Quantum Electron. **QE-9**, 919 (1973).
[7] R. Kazarinov and C. Henry, IEEE J. Quantum Electron. **QE-21**, 144 (1985).
[8] S. John, Phys. Rev. Lett. **58**, 2486 (1987).
[9] E. Yablonovitch, Phys. Rev. Lett. **58**, 2059 (1987).
[10] J. D. Joannopoulos, R. D. Meade, and J. N. Winn, *Photonic Crystals* (Princeton University Press, Princeton, 1995).
[11] W. M. Robertson and G. Arjavalingam, Phys. Rev. Lett. **68**, 2023 (1992).
[12] S. Y. Lin *et al.*, Nature (London) **394**, 251 (1998).
[13] R. D. Meade, A. Devenyi, J. D. Joannopoulos, O. L. Alerhand, D. A. Smith, and K. Kash, J. Appl. Phys. **75**, 4753 (1994).
[14] J. S. Foresi *et al.*, Opt. Photonics News **8**, 48 (1997).
[15] J. Chen, H. A. Haus, S. Fan, P. R. Villeneuve, and J. D. Joannopoulos, J. Lightwave Technol. **14**, 2575 (1996).
[16] M. Kanskar, P. Paddon, V. Pacradouni, R. Morin, A. Busch, J. F. Young, S. R. Johnson, J. Mackenzie, and T. Tiedje, Appl. Phys. Lett. **70**, 1438 (1997).
[17] J. E. Sipe, J. Opt. Soc. Am. B **4**, 481 (1987).
[18] M. Born and E. Wolf, *Principles of Optics* (Pergamon, Oxford, 1959).
[19] R. H. Ritchie, Phys. Rev. **106**, 874 (1957).
[20] A. R. Cowan, P. Paddon, and Jeff F. Young (unpublished).
[21] P. Paddon and Jeff F. Young, Opt. Lett. **23**, 1529 (1998).
[22] In Fig. 2, the resultant energy splitting of the nondegenerate states at the TE gap is quite small, less than the width of the lines.
[23] Jeff F. Young, P. Paddon, V. Pacradouni, S. Johnson, and T. Tiedje, in *Proceedings of the 1998 Workshop on Future Trends in Microelectronics, Embiez France*, edited by S. Luryi, J. Xu, and A. Zaslavsky (John Wiley and Sons, New York, 1999).
[24] V. Pacvadouni, A. R. Cowan, W. J. Mandeville, P. Paddon, S. R. Johnson, and Jeff F. Young (unpublished).